frontiers | Frontiers in Marine Science

ORIGINAL RESEARCH
published: 06 May 2022
doi: 10.3389/fmars.2022.897729

# Rapidly Increasing Artificial Iodine Highlights Pathways of Iceland-Scotland Overflow Water and Labrador Sea Water

*Maxi Castrillejo[1,2*], Núria Casacuberta[1,3,4], Christof Vockenhuber[1] and Pascale Lherminier[5]*

[1] Laboratory of Ion Beam Physics, ETH Zurich, Zurich, Switzerland, [2] Department of Physics, Imperial College London, London, United Kingdom, [3] Institute of Biogeochemistry and Pollutant Dynamics, Environmental Physics, ETH Zurich, Zurich, Switzerland, [4] Department of Environmental Systems Science, ETH Zurich, Zurich, Switzerland, [5] Ifremer, Univ. Brest, CNRS, IRD, Laboratoire d' Océanographie Physique et Spatiale, IUEM, Plouzané, France

OPEN ACCESS

**Edited by:**
Jixin Qiao,
Technical University of Denmark,
Denmark

**Reviewed by:**
Luyuan Zhang,
Institute of Earth Environment (CAS),
China
Ala Aldahan,
United Arab Emirates University,
United Arab Emirates

***Correspondence:**
Maxi Castrillejo
m.castrillejo-iridoy@imperial.ac.uk

**Specialty section:**
This article was submitted to
Ocean Observation,
a section of the journal
Frontiers in Marine Science

**Received:** 16 March 2022
**Accepted:** 07 April 2022
**Published:** 06 May 2022

**Citation:**
Castrillejo M, Casacuberta N,
Vockenhuber C and Lherminier P
(2022) Rapidly Increasing Artificial
Iodine Highlights Pathways of
Iceland-Scotland Overflow Water
and Labrador Sea Water.
Front. Mar. Sci. 9:897729.
doi: 10.3389/fmars.2022.897729

Iceland-Scotland Overflow Water (ISOW) and Labrador Seawater (LSW) are major water masses of the lower Atlantic Meridional Overturning Circulation (AMOC). Therefore, the investigation of their transport pathways is important to understand the structure of the AMOC and how climate properties are exported from the North Atlantic to lower latitudes. There is growing evidence from Lagrangian model simulations and observations that ISOW and LSW detach from boundary currents and spread off-boundary, into the basin interior in the Atlantic Ocean. Nuclear fuel reprocessing facilities of Sellafield and La Hague have been releasing artificial iodine ($^{129}I$) into the northeastern Atlantic since the 1960ies. As a result, $^{129}I$ is supplied from north of the Greenland-Scotland passages into the subpolar region labelling waters of the southward flowing lower AMOC. To explore the potential of $^{129}I$ as tracer of boundary and interior ISOW and LSW transport pathways, we analyzed the tracer concentrations in seawater collected during four oceanographic cruises in the subpolar and subtropical North Atlantic regions between 2017 and 2019. The new tracer observations showed that deep tracer maxima highlighted the spreading of ISOW along the flanks of Reykjanes Ridge, across fracture zones and into the eastern subpolar North Atlantic supporting recent Lagrangian studies. Further, we found that $^{129}I$ is intruding the Atlantic Ocean at unprecedented rate and labelling much larger extensions and water masses than in the recent past. This has enabled the use of $^{129}I$ for other purposes aside from tracing ISOW. For example, increasing tracer levels allowed us to differentiate between newly formed $^{129}I$-rich LSW and older vintages poorer in $^{129}I$ content. Further, $^{129}I$ concentration maxima at intermediate depths could be used to track the spreading of LSW beyond the subpolar region and far into subtropical seas near Bermuda. Considering that $^{129}I$ releases from Sellafield and La Hague have increased or levelled off during the last decades, it is very likely that the tracer invasion will continue providing new tracing opportunities for $^{129}I$ in the near future.

**Keywords: artificial radionuclides, $^{129}I$, ISOW, LSW, AMOC, iodine, ocean circulation**

## INTRODUCTION

The water circulation in the subpolar North Atlantic (SPNA) plays a key role on the conduit of greenhouse gases and other climate properties from the sea surface down to the ocean interior (e.g., Perez et al., 2018). Climate signals are then exported southward through the lower limb of the Atlantic Meridional Overturning Circulation (AMOC). This limb is mainly composed by the Labrador Sea Water (LSW) and the two dense overflows supplied from the Nordic Seas, namely, the Denmark Strait Overflow Water (DSOW) and the Iceland-Scotland Overflow Water (ISOW). The circulation of DSOW is being investigated in the Labrador Sea and further south off the north American shore using time series observations of artificial iodine ($^{129}$I) that started in the early 1990's (Smith et al., 2005; Orre et al., 2010; Smith et al., 2016). The focus of this study is on exploring the potential of $^{129}$I to trace the complex pathways of ISOW and LSW in the SPNA and further south into the subtropical North Atlantic Ocean.

Among the two water masses, ISOW is the less well understood due to its complex transport pathways, temporal variability and strong mixing with contiguous water bodies. The historical ISOW circulation scheme describes a single boundary transport (magenta solid lines in **Figure 1**). In that depiction, ISOW spills from the Nordic Seas into the SPNA through the sills between Iceland and Scotland (Hansen and Østerhus, 2007; Beaird et al., 2013), and follows a westward journey along the perimeter of the Iceland Basin passing primarily through the Charlie – Gibbs Fracture Zone into the Irminger Sea (Saunders, 1994; Bower and Furey, 2017). Then ISOW turns northward as part of the boundary current in the western flank of Reykjanes Ridge and eventually joins the southward flowing Deep Western Boundary Current in the east Greenland Slope (Dickson and Brown, 1994; Schott et al., 1999). However, there is growing evidence from numerical simulations and field observations (e.g., Zou et al., 2020) to portray a more complex circulation scheme in which ISOW travels, more often than previously thought, off boundary currents (magenta dotted lines in **Figure 1**). For example, a number of Lagrangian floats deployed at the Reykjanes Ridge and programmed to drift at ISOW levels showed trajectories that detach from the boundary current to travel westward into the Irminger Sea, southward along the flanks of the Mid Atlantic Ridge, or eastward to the afar West European Basin (Bower et al., 2002; Lankhorst and Zenk, 2006; Xu et al., 2010; Zou et al., 2017; Racapé et al., 2019; Zou et al., 2020).

Along the journey in the SPNA, ISOW mixes with other water masses, especially with central waters carried by the North Atlantic Current and LSW (Yashayaev et al., 2007; Beaird et al., 2013; Devana et al., 2021). LSW forms by winter convection in the Labrador Sea and Irminger Sea and constitutes the major intermediate water mass spreading across the North Atlantic (Clarke and Gascard, 1983; Yashayaev et al., 2007; Piron et al., 2017). The transport pathways of LSW are better known, yet similar to ISOW, drifting buoy observations indicate strong recirculation of this water mass eastward into interior basins (e.g., Bower et al., 2009). The number of floats might still be insufficient, especially for ISOW, but the emerging views are already compelling for the export of climate anomalies and suggest that further investigation is needed to provide a better understanding of the structure of the AMOC (Bower et al., 2019).

Radionuclide transient tracers are valuable tools to complement the information obtained from floats and other physical observations. Hydrographic tracer distributions integrate past circulation as if floats were released in great number. A strong tracer candidate for the investigation of the overflows and LSW is $^{129}$I, which is released by the nuclear fuel reprocessing industry into the surface seawater in the North Sea region and eventually transported into the SPNA (Yiou et al., 1994; Edmonds et al., 2001; Alfimov et al., 2004; Smith et al., 2005; Smith et al., 2011; Alfimov et al., 2013; Gómez-Guzmán et al., 2013; He et al., 2013a; He et al., 2013b; Smith et al., 2016; Casacuberta et al., 2018; Castrillejo et al., 2018; Vivo-Vilches et al., 2018; Wefing et al., 2018). This tracer has already been successfully employed to identify and follow DSOW between the Irminger Sea and Bermuda based on its increasing concentrations that can be measured with high sensitivity, i.e., million atoms per liter of seawater (Smith et al., 2005; Smith et al., 2016). However, measurements of $^{129}$I conducted prior to Castrillejo et al. (2018) and this study indicated that tracer levels in ISOW and LSW were not large enough to allow the clear differentiation of these water masses in the North Atlantic (Santschi et al., 1996; Edmonds et al., 2001). On the other hand, numerical modelling (Orre et al., 2010) projects a rise in $^{129}$I concentrations at depths typically occupied by ISOW in the eastern SPNA in response to increased radionuclide discharge rates in recent decades. A glimpse of such tracer increase in ISOW was captured for the first time in 2014 in the Iceland Basin (Castrillejo et al., 2018). Additionally, the $^{129}$I time series conducted in the AR7W line show increasing tracer concentrations in LSW between 1993 and present (Smith et al., 2005; Orre et al., 2010; Smith et al., 2016). These results imply that if $^{129}$I was to continue increasing, the tracer could potentially reveal ISOW and LSW transport pathways in parts of the North Atlantic where their identification can be challenging if using properties such as salinity and temperature alone.

The aim of this work is to further explore the potential of $^{129}$I to trace ISOW and LSW transport pathways in the near future. To that end, we measured $^{129}$I from over 200 seawater samples collected across the subpolar and subtropical North Atlantic between 2017 and 2019. The new $^{129}$I dataset captured deep tracer maxima associated with density, salinity and potential temperatures expected for ISOW. Using $^{129}$I depth profiles we were able to provide an independent validation of ISOW pathways being redrawn by Lagrangian studies. Specifically, we observed ISOW spreading along the boundary current in the eastern flank of the Reykjanes Ridge, over the ridge through the Bight Fracture Zone and off the boundary current following interior routes into the Iceland Basin and the West European Basin. The comparison of the new $^{129}$I dataset to earlier distributions shows that tracer concentrations increased notably in recent years, allowing for the first time the straightforward tracking of ISOW by using this tracer. Further, we found that $^{129}I$ increased at an unprecedented rate after 2014 intruding other water masses in the SPNA. For example, $^{129}I$ allows distinguishing between different vintages of LSW in the SPNA and following the southward export of LSW through interior pathways into the subtropical region.

## SOURCES OF $^{129}I$

The presence of $^{129}I$ in the North Atlantic is dominated by authorized, marine liquid discharges occurring since the 1960ies until present from the nuclear fuel reprocessing plants of La Hague into the English Channel and Sellafield into the Irish Sea (**Figure 1**). The $^{129}I$ discharges have been documented over the past decades in reports of the European OSPAR commission, the Environmental Agency of the UK, or by companies running the nuclear installations (e.g., OSPAR, 2015; UK Environmental Agency, 2015). The two facilities alone have discharged more than 6000 kg of $^{129}I$ to regional waters (He et al., 2013a), which is well above the ~90 kg globally dispersed in the 1950ies/60ies as fallout through atmospheric nuclear weapon tests (Wagner et al., 1996; Raisbeck and Yiou, 1999; Hou, 2004). The combined marine discharge rate of the two reprocessing plants increased gradually from < 1 kg/yr to about 100 kg/yr in the first 20 years, then escalated through the 1990s to peak at > 350 kg/yr in the early 2000s and remained above 200 kg/yr in the most recent part (**Figure 1**). The long residence time of iodine in the ocean water column [over 300,000 yr (Broecker and Peng, 1982; Wong, 1991)] and the limited interaction with organic particles in the photic layer (Schink et al., 1995) suggest that iodine behaves almost conservatively in the ocean. This conservative behavior is confirmed by the long-distance transport of marine $^{129}I$ discharges (e.g. Santschi et al., 1996; Smith et al., 2016) through the North Sea, the Nordic Seas, the Arctic Ocean and as far as the subtropical North Atlantic (see the routes schematically depicted in **Figure 1**). Consequently, the $^{129}I$ content in waters circulating between the point of discharge and the Arctic Ocean can be 6 to 12 orders of magnitude above the natural levels (< 0.1 $\times 10^7$ at/kg; atoms per kilogram of seawater) (Snyder et al., 2010) or weapon tests fallout levels (<< 10 $\times 10^7$ at/kg) (Edmonds et al., 2001). Further transport and mixing of waters from the Arctic, North Sea and northeast Atlantic leads to the entrainment of $^{129}I$ in different water masses and streams within the Nordic Seas. The overall result is a supply of *northern waters* with $^{129}I$ in the range of $\times 10^8$ - $\times 10^{10}$ at/kg *via* the Greenland – Scotland passages into the SPNA. These northern waters mix with northward flowing *southern waters* originating from lower latitudes (e.g., tropical and South Atlantic). The lower latitude waters may present small impacts of reprocessing marine discharges due to shallow water recirculation in the North Atlantic (He et al., 2013b), but they are generally affected by weapon tests alone and thus carry 10 to 10,000 times less $^{129}I$ than the northern waters (Castrillejo et al., 2018).

## METHODS

### Sample Collection

Sea water samples were collected strategically to investigate the pathways of the southward lower AMOC in the subpolar and subtropical North Atlantic Ocean between 2017 and 2019. Colored dots in **Figure 1** show the locations visited during the four cruises: i) the Iceland Basin and the West European Basin on board the Dutch *R/V Pelagia* during the PE424 (PE) cruise in July-August 2017; ii) between Lisbon, Portugal, and Cape

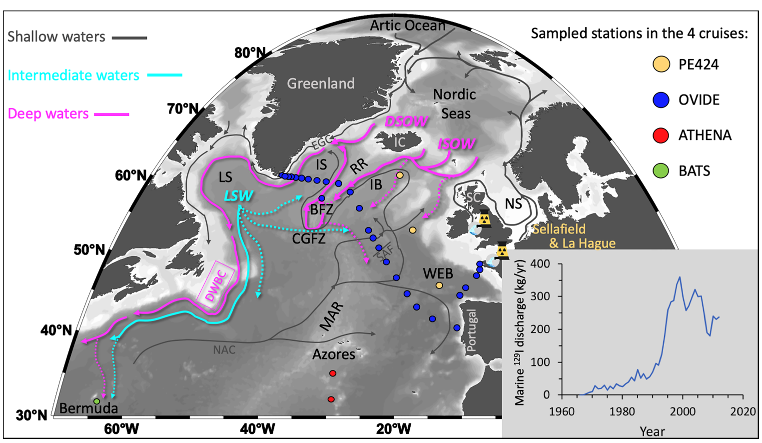


**FIGURE 1** | Sampling sites during the four cruises (PE424, OVIDE, ATHENA and BATS), the combined $^{129}I$ marine discharge from the nuclear reprocessing plants of Sellafield and La Hague since the 1960s until the recent past (e.g. OSPAR, 2015; UK Environmental Agency, 2015), and the schematic circulation adapted from Daniault et al. (2016) to highlight boundary (solid lines) and interior (dotted lines) pathways of ISOW, LSW and DSOW. Acronyms in figure: Bight Fracture Zone, (BFZ); Charlie – Gibbs Fracture Zone, (CGFZ); Denmark Strait Overflow Water, (DSOW); Deep Western Boundary Current, (DWBC); East Greenland Current, (EGC); Iceland Basin, (IB); Iceland, (IC); Iceland Scotland Overflow Water, (ISOW); Irminger Sea, (IS); Labrador Sea, (LS); Labrador Sea Water, (LSW); Mid Atlantic Ridge, (MAR); North Atlantic Current, (NAC); North Sea, (NS); Reykjanes Ridge, (RR); Sub-Arctic Front, (SAF); Scotland, (SC); and West European Basin, (WEB).

Farewell, Greenland, on board the French *R/V Thalassa* during OVIDE (OV) cruise in June-July 2018; iii) south of the Azores Archipelago in the tropical North Atlantic during ATHENA (ATH) cruise on board the German *R/V Meteor* in October 2018; and iv) the Bermuda Atlantic Time Series (BATS) station on board the North American *R/V Atlantic Explorer* in June 2019.

In all cruises surface seawater was collected using a surface pump and the water column was sampled using rosettes equipped with Niskin bottles and CTD oxygen-conductivity-temperature-pressure sensors. The seawater was transferred to 500 mL dark plastic bottles after rinsing them 3 times with seawater. Samples were either processed onboard or at land-based laboratories at ETH-Zurich.

## Radiochemistry and AMS Measurement of Iodine Isotopes

Iodine was extracted from about 400 mL of seawater at ETH-Zurich following the methods described in Castrillejo et al. (2018). Each sample was spiked with about 1.5 mg of Woodward stable iodine carrier ($^{127}$I). All iodine in seawater was oxidized to iodate upon addition of 2% $Ca(ClO)_2$ and then reduced to iodide by adding $Na_2S_2O_5$ and 1M of $NH_3O{\bullet}HCl$ solution. Columns filled with DOWEX® 1X8 ion exchange resin were conditioned with deionized water and diluted 0.5 M $KNO_3$ solution. The loading of the sample in the column was followed by the elution of all the iodine by adding 2.25 M $KNO_3$ solution and precipitation as AgI using $AgNO_3$. The precipitate was mixed with about 4 mg of Ag and pressed into cathodes for Accelerator Mass Spectrometry (AMS). Replicates of a seawater sample (n=11) were conducted to check internal consistency. Blanks (n=48) were prepared using deionized water and treated following the same procedure as for the seawater samples.

The calculation of $^{129}$I concentrations was done based on the measured $^{129}$I/$^{127}$I ratio and the well-known amounts of $^{127}$I carrier spiked to each sample. The $^{129}$I/$^{127}$I atom ratios were measured using the compact 0.5 MV Tandy AMS system at ETH-Zurich (Vockenhuber et al., 2015). The $^{129}$I/$^{127}$I ratios were normalized with the ETH-Zurich in-house standard D22 with nominal $^{129}$I/$^{127}$I of $(50.35 \pm 0.16) \times 10^{-12}$ (Christl et al., 2013) and secondary standards with ratios of $5 \times 10^{-12}$ that are linked to D22. Blanks presented (2-8) $\times 10^5$ atoms/kg of $^{129}$I, corresponding to 1-5% of the total $^{129}$I measured in seawater samples.

# RESULTS

## $^{129}$I Concentrations in the SPNA Between 2017 and 2019

All measured $^{129}$I concentrations are reported in **Table S1** along with temperature, salinity and dissolved oxygen data. In the SPNA we sampled 17 depth profiles which are represented in **Figure 2**. And, collected additionally 10 surface and 6 near bottom samples which are not shown in **Figure 2**.

The $^{129}$I concentrations in all seawater samples ranged between $(0.05 \pm 0.05) \times 10^7$ at/kg and $(275 \pm 4) \times 10^7$ at/kg. The lowest $^{129}$I concentrations represent natural waters without anthropogenic influence or that contain a small amount of nuclear weapon test fallout. On the other end, the highest $^{129}$I concentrations indicate a strong influence of marine discharges from Sellafield and La Hague. **Figure 2** displays a map of $^{129}$I depth profiles along the OVIDE line (**Figure 2A**) which are arranged in three panels from low- (**Figure 2B**), mid- (**Figure 2C**), to high- (**Figure 2D**) tracer concentrations. The $^{129}$I concentrations generally increased from east to west. We found the lowest values at depths greater than 3000 m in the West European Basin (OV7-33, **Figure 2B**). The Iceland Basin (OV43-104, **Figure 2C**) represented a region of transition where we began to observe higher $^{129}$I concentrations in the intermediate range of (10 - 40) $\times 10^7$ at/kg. The bottom layer of the Irminger Sea and the east Greenland shelf (OV76-93, **Figure 2D**) presented the highest $^{129}$I concentrations in the order of $\times 10^8$ - $\times 10^9$ at/kg. The $^{129}$I concentrations from PE stations were similar to those found in the Iceland Basin and the West European Basin during OVIDE (**Figure 2C**).

All acronyms used hereinafter to denote water masses, currents and geographic locations are listed in **Table 1** and explained in the figure captions.

## Relationship Between $^{129}$I and Water Masses in the SPNA

To discuss the transport pathways of ISOW and LSW on basis of $^{129}$I concentrations it is first necessary to understand how tracer

**TABLE 1** | Acronyms used to denote water masses, currents and geographic locations.

| | | | |
|---|---|---|---|
| BATS | Bermuda Atlantic Time Series | MC | Maury Channel |
| BFZ | Bight Fracture Zone | NAC | North Atlantic Current |
| CGFZ | Charlie – Gibbs Fracture Zone | NADW | North Atlantic Deep Water |
| DSOW | Denmark Strait Overflow Water | NEADW | North East Atlantic Deep Water |
| DWBC | Deep Western Boundary Current | NS | North Sea |
| EGC | East Greenland Current | PIW | Polar Intermediate Waters |
| ENACW | Eastern North Atlantic Central Water | RP | Rockall Plateau |
| IB | Iceland Basin | RT | Rockall Through |
| IC | Iceland | RR | Reykjanes Ridge |
| ISOW | Iceland Scotland Overflow Water | SAF | Sub-Arctic Front |
| IS | Irminger Sea | SC | Scotland |
| LS | Labrador Sea | SPMW | Subpolar Mode Waters |
| LSW | Labrador Sea Water | WEB | West European Basin |
| MAR | Mid Atlantic Ridge | | |

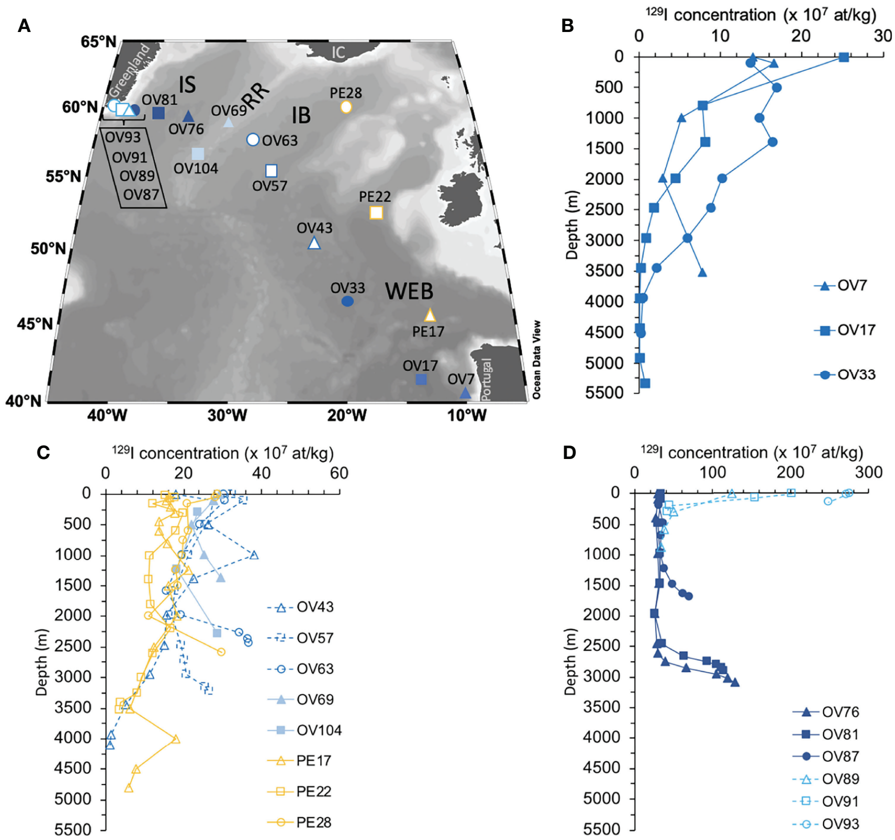


**FIGURE 2** | **(A)** Map of $^{129}$I depth profiles displayed from **(B)** low-, **(C)** mid-, to **(D)** high- concentrations. The legends include all stations sampled during the PE424 cruise in 2017 (PE) and the OVIDE cruise in 2018 (OV). Acronyms in figure: Iceland Basin, (IB); Iceland, (IC); Irminger Sea, (IS); Reykjanes Ridge, (RR); and West European Basin, (WEB).

concentrations relate to the water mass structure. Here we focus on OVIDE data because the location of the section is representative for $^{129}$I concentrations and water masses that reign in the SPNA (OVIDE+PE), and that are to large extent, present in lower latitudes of the Atlantic Ocean (BATS+ATH). Firstly, we plot the radionuclide concentrations from the OVIDE line versus potential temperature (θ) and salinity (S) in $\theta$ - $S$ diagrams (**Figure 3A**). The water mass endmembers (diamond symbols in **Figure 3A**) are chosen based on the most recent water mass classification for the OVIDE line (García-Ibáñez et al., 2018). Secondly, we represent the zonal distribution of $^{129}$I with the overlaid water mass structure (**Figure 3B**). The water mass structure was inferred from the $\theta$ - $S$ diagrams (**Figure 3A**) and zonal distributions of S, θ and $O_2$ (**Figure S1**).

The $\theta$ - $S$ diagrams (**Figure 3A**) show the purest ISOW east of the Reykjanes Ridge characterized by salinity above 34.95, potential temperature of 2-3°C and density in the range of 27.85 – 27.90 kg/m$^3$. In the SPNA, ISOW entrains and mixes mainly with LSW (McCartney and Talley, 1982; Yashayaev et al., 2007) to form the upper North East Atlantic Deep Water ($NEADW_U$). The lower branch ($NEADW_L$) has less ISOW and a larger contribution of Lower Deep Water from Antarctica (van Aken, 2000a). The lower and upper branches of NEADW fall roughly in a similar density range as for ISOW but are comparably fresher and colder. West of Reykjanes Ridge ISOW further mixes with underlying DSOW and overlying LSW. Compared to ISOW, DSOW presents a lower salinity (~ 34.90) and potential temperature (< 2°C), and a density greater than 27.90 kg/m$^3$. The LSW present in the Irminger Sea is fresher (S < 34.90), warmer (θ ~ 3°C) and lighter (27.75 kg/m$^3$) than the two overflows. This LSW probably includes waters formed during strong winter convection events in 2013-2014 that have been further renewed with LSW produced during 2015-2017 in the Labrador Sea and the Irminger Sea (Yashayaev and Loder, 2016; Piron et al., 2017). For simplicity we will differentiate between this LSW ($LSW_{new}$) and use the term $LSW_{old}$ for the LSW that left the convection regions and has travelled further (south)east in the SPNA suffering significant entrainment and mixing during its downstream journey. Other water masses in the SPNA include: the southward flowing Subpolar Mode Waters (SPMWs, other than LSW) that result from cooling and freshening of Eastern North Atlantic Central Water (ENACW) through convection events in the SPNA; Polar Intermediate Water (PIW), the freshest and coldest water originating from

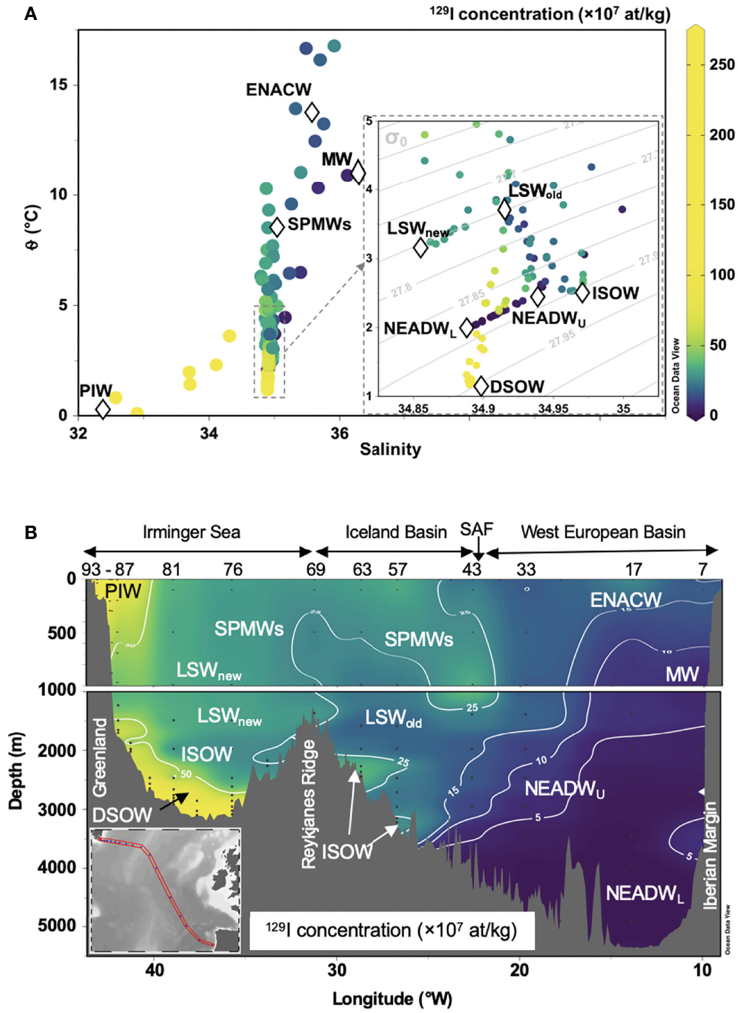


**FIGURE 3** | Relationship of $^{129}$I with water masses in the SPNA. **(A)** Potential temperature (θ) – salinity diagrams. The color bar indicates the $^{129}$I concentrations. **(B)** Zonal section of $^{129}$I concentrations. The color coding is the same as for **(A)**. The acronyms of the water masses shown in **(A)** are also represented in **(B)**. Data correspond to the OVIDE cruise in 2018. Acronyms in figure: Denmark Strait Overflow Water, (DSOW); East North Atlantic Central Water, (ENACW); Iceland Scotland Overflow Water, (ISOW); Labrador Sea Water, (LSW); Mediterranean Water, (MW); North East Atlantic Deep Water, (NEADW, lower and upper); Polar Intermediate Water, (PIW); Sub-Arctic Front, (SAF); Subpolar Mode Water, (SPMW).

the Arctic Ocean; and the Mediterranean Water (MW) characterized by the highest salinity along the OVIDE line.

The vertical distribution of $^{129}$I along the OVIDE section (**Figure 3B**) allows the straightforward distinction between northern and southern origin water masses. Waters of northern origin generally presented $^{129}$I concentrations above 20 $\times 10^7$ at/kg and occupied the region west of 22.5°W which is geographically delimited by the position of the Sub-Arctic Front. In this group we observe ISOW with $^{129}$I concentrations in the (25-40) $\times 10^7$ at/kg range, PIW along the east Greenland shelf carrying the highest $^{129}$I concentrations (> 100 $\times 10^7$ at/kg), the core of DSOW filling the bottom of the Irminger Sea with $^{129}$I concentrations slightly above 100 $\times 10^7$ at/kg, and LSW and SPMWs with concentrations in the range of (15 – 40) $\times 10^7$ at/kg. $LSW_{new}$ filling the Irminger Sea water column carries more $^{129}$I than the older LSW that is present east of Reykjanes Ridge. Southern waters dominated the region east of the Sub-Arctic Front and carried little $^{129}$I (< 15 $\times 10^7$ at/kg) in comparison to northern waters. Because of this reason, the identification of ISOW and LSW was easily accomplished by searching for $^{129}$I spikes at deep and intermediate depths (e.g., eastern flank of Reykjanes Ridge in **Figure 3B**), even when these water masses were difficult to distinguish by using S, θ and $O_2$ alone (**Figure S1**).

# DISCUSSION

## Observed ISOW Pathways in 2017-2018

Here we provide an independent means of validating transport pathways of ISOW. Our approach is based on the identification of deep, high $^{129}$I concentrations (> 15 $\times 10^7$ at/kg) captured at the layer with 27.85 – 27.90 kg/m$^3$ potential density, S >34.95 and θ of 2-3°C. We focus on cases where there is a large $^{129}$I concentration gradient between ISOW and surrounding water masses. These conditions are met in the Reykjanes Ridge, Iceland Basin and the West European Basin, but not in the Irminger Sea because there the $^{129}$I concentrations of ISOW are surpassed by higher tracer amounts carried by the underlying DSOW.

We found seven $^{129}$I depth profiles from OVIDE and PE424 cruises that captured the mentioned deep tracer spike in 2017/2018 (yellow and blue data in Figs. 4A-4C). Station positions are shown in **Figure 4D**. The largest $^{129}$I spike, of (36.8 ± 0.8) $\times 10^7$ at/kg, was measured at 2440 m depth in station OV63 located in the eastern flank of Reykjanes Ridge (**Figure 4A**). The result is consistent with a substantial amount of ISOW following the counterclockwise boundary current in the Iceland Basin towards the ridge (e.g., Daniault et al., 2016). The crossing of ISOW from the Iceland Basin into the Irminger Sea occurs primarily *via* fracture zones (Petit et al., 2018). Traditionally it was thought that the principal origin of ISOW found in the boundary current along the western flank of the Reykjanes Ridge (Daniault et al., 2016) was the Charlie Gibbs Fracture Zone. However, there is growing evidence from modelled and observed float trajectories that Bight Fracture Zone is a very important pathway of ISOW into the western flank of the ridge (Bower et al., 2002; Xu et al., 2010; Zou et al., 2017; Zou et al., 2020). For example, some floats deployed at ISOW densities in the Bight Fracture Zone (Bower et al., 2002; Lankhorst and Zenk, 2006; Zou et al., 2017) have described northward flows connecting with the boundary current while the majority of RAFOS and Deep Argo floats released at the Charlie Gibbs Fracture Zone followed west-northwest interior pathways or took a southward direction along the Mid Atlantic Ridge (Racapé et al., 2019; Zou et al., 2020). To check whether there was ISOW at the Bight Fracture Zone during OVIDE 2018 we collected a near-bottom seawater sample at 2280 m depth in station OV104 (**Figure 4A**). The unequivocal $^{129}$I spike [(28.8 ± 0.4) $\times 10^7$ at/kg] was observed again indicating the presence of ISOW that was warmer and lighter than the one found in the eastern flank of Reykjanes Ridge (**Table S1**).

In the eastern North Atlantic, $^{129}$I observations suggest that several veins of ISOW spread following interior routes. The $^{129}$I peak of about (26 – 30) $\times 10^7$ at/kg was easily identified in near bottom waters collected at stations PE28 and OV57 (**Figure 4B**)

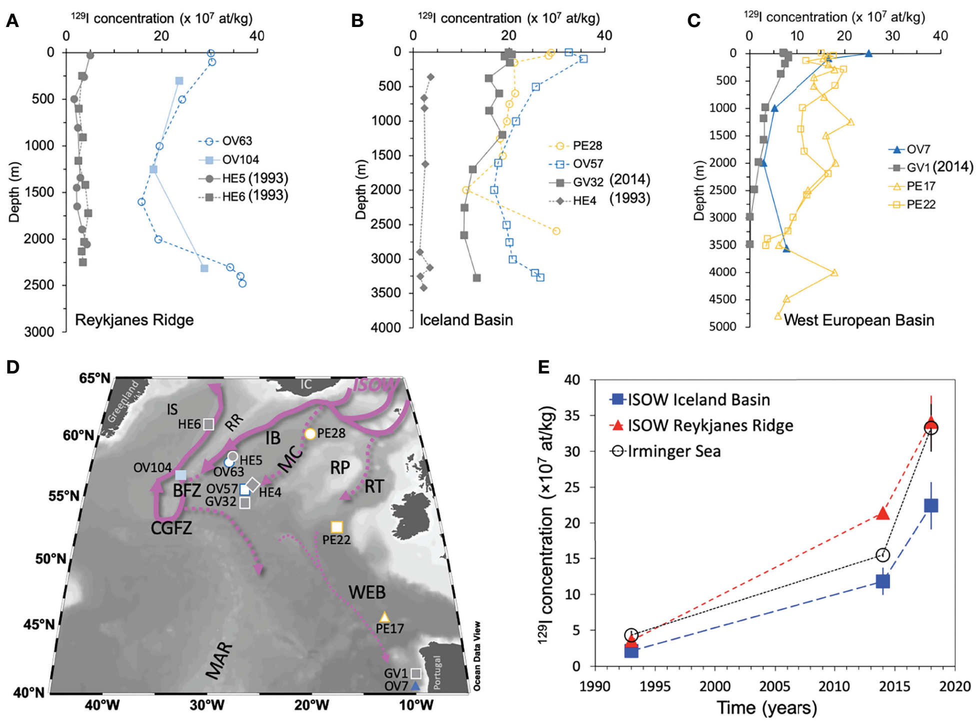


**FIGURE 4** | $^{129}$I in the Northeastern Atlantic Ocean. Depth profiles of $^{129}$I obtained during OVIDE cruise in 2018 (OV, blue) and the PE424 cruise in 2017 (PE, yellow) at **(A)** Reykjanes Ridge, **(B)** the Iceland Basin, and **(C)** the West European Basin, are represented and compared to nearby depth profiles available in the literature (grey profiles): HE sites measured in 1993 by Edmonds et al. (2001) and GV sites from the GEOVIDE cruise in 2014 (Castrillejo et al., 2018) revisited during OVIDE in 2018. **(D)** Map showing the stations (*) and boundary (solid lines) and interior pathways of ISOW (dotted lines). *Stations GV1 and GV32 were at the same location as OV7 and OV57 respectively. **(E)** Temporal evolution of mean $^{129}$I concentrations in ISOW at the Reykjanes Ridge, Iceland Basin and the Irminger Sea. Data used for **(E)** are summarized in **Table S2**. Acronyms in figure: Bight Fracture Zone, (BFZ); Charlie – Gibbs Fracture Zone, (CGFZ); Iceland Basin, (IB); Iceland, (IC); Iceland Scotland Overflow Water, (ISOW); Irminger Sea, (IS); Maury Channel, (MC); Mid Atlantic Ridge, (MAR); Reykjanes Ridge, (RR); Rockall Plateau, (RP); Rockall Through, (RT); and West European Basin, (WEB).

pointing to ISOW passages near Maury Channel in the eastern Iceland Basin (**Figure 4D**). This result agrees with modelled and deployed float trajectories (Xu et al., 2010; Zou et al., 2017; Zou et al., 2020) as well as with hydrographic surveys (Daniault et al., 2016), although the limited sampling resolution in this study does not allow confirming if ISOW captured at PE28 and OV57 corresponds to a southward branch detached from the boundary current (as in Zou et al., 2017) or to water that recirculated eastward from the Mid Atlantic Ridge. In comparison to the Iceland Basin, in the West European Basin deep tracer maxima were more diluted due to greater mixing of ISOW with southern components of NEADW (**Figure 4C**). Yet, one could still use $^{129}$I to distinguish ISOW contributions to NEADW even when the two water masses display similar salinities and potential temperatures (García-Ibáñez et al., 2018). For example, PE22 captures a small peak of $^{129}$I ((16.6 ± 0.2) ×$10^7$ at/kg) at 2200 m depth in the intersect between Rockall Through and the West European Basin consistent with a small southward flow of ISOW (Sherwin et al., 2008; Chang et al., 2009; Zou et al., 2017). And further south and below 3000 m depth, station PE17 and OV7 presented tracer peaks of (17.9 ± 0.2) ×$10^7$ at/kg and (7.8 ± 0.2) ×$10^7$ at/kg, respectively. These tracer maxima can only be explained by the lateral advection of dense overflows like ISOW into the West European Basin in the absence of other sources of $^{129}$I at low latitudes (van Aken, 2000a; Fleischmann et al., 2001; Zou et al., 2017; Xu et al., 2018), but their travel path is still unrevealed.

## Temporal Evolution of $^{129}$I in ISOW

In the 1990s sufficient $^{129}$I was found only in DSOW while the tracer content was close to the natural background in other waters of the North Atlantic Ocean (Santschi et al., 1996; Edmonds et al., 2001; Smith et al., 2005). Thus, when did $^{129}$I begin to reveal ISOW pathways? To answer this question, we compare the $^{129}$I depth profiles from 2017-2018 to previous observations (grey profiles) in the SPNA (**Figure 4**). Edmonds et al. (2001) reported the first $^{129}$I depth profiles (stations labelled as 'HE' in **Figure 4D**) in the eastern (HE5) and western (HE6) flanks of the Reykjanes Ridge and southwest of the Rockall Plateau in the Iceland Basin (HE4) for samples collected in 1993. Their $^{129}$I profiles (**Figures 4A, B**) showed very low tracer concentrations throughout the water column. On the contrary, the overflow water begun to carry sufficient $^{129}$I in the Iceland Basin (station GV32) in 2014 (Castrillejo et al., 2018). And it was not until 2018 that a strong tracer signal unraveled the passage of ISOW in the Iceland Basin (OV 57) and other parts of the SPNA.

To provide a more comprehensive view on the temporal evolution of $^{129}$I in ISOW, we calculated the mean tracer concentrations using all available measurements in the overflow found east of Greenland and west of the West European Basin. We exclude the West European Basin from the calculations because tracer data are insufficient to infer any temporal trend in that region. West of the West European Basin, $^{129}$I observations are also limited (**Table S2**), yet **Figure 4E** convincingly shows a clear increase in tracer values between 1993 and 2018. Whether tracer concentrations increased linearly or stepwise cannot be inferred based on the limited tracer measurements. But it is clear that during the 25-year time period the $^{129}$I concentration in ISOW was multiplied 10 times on average, from lower than 5 ×$10^7$ at/kg in the 1990s to higher than 30 ×$10^7$ at/kg in the 2010s. Half of the $^{129}$I increase occurred between 1993 and 2014 while tracer levels doubled in the short time span between 2014 and 2018. Will $^{129}$I continue labelling ISOW? The answer is: very likely yes. It is reasonable to think that in comparison to present, future ISOW will carry similar quantities of $^{129}$I, or more, because of two reasons: firstly, the repeated $^{129}$I measurements in DSOW show that its tracer content is still rising (see **Figure 3** in Smith et al., 2016); secondly, the marine radionuclide discharge from the reprocessing facilities in Europe has either increased or levelled off during the last decades (see *Sources of $^{129}$I*). The expected implications are that $^{129}$I will stand out in ISOW and that the tracer has potential to shed light on time scales of ISOW circulation between the source and the SPNA and further downstream provided there is a continuation of $^{129}$I observations to extend the so far limited time series displayed in **Figure 4E**.

## Spreading of $^{129}$I in LSW

To investigate whether $^{129}$I was increasing rapidly in other water masses of the SPNA we compared the vertical distribution of $^{129}$I along the OVIDE line between 2014 and 2018 (**Figure 5A**). The colored dots and contour lines (in spite of the excessive interpolation) show that $^{129}$I concentrations in the region occupied by northern waters were in all cases higher (i.e., positive values) in 2018 than in 2014, while southern waters showed small differences in the tracer field (< 5 ×$10^7$ at/kg). The influence of increased $^{129}$I releases from the European reprocessing plants (see *Sources of $^{129}$I*) is most notorious in the area delimited by difference contour lines of (5-10) ×$10^7$ at/kg. Apart from the overflows and shallow waters, the area comprised by these contour lines is mainly filled by LSW. In **Figure 3** we showed that it is possible to distinguish young LSW vintages in the Irminger Sea by their higher $^{129}$I concentrations from the tracer poorer and older LSW that spread (south)eastward passing the Reykjanes Ridge. This is consistent with the formation process of LSW that incorporates $^{129}$I-rich Arctic-origin fresh water during convective events in the Labrador Sea (van Aken, 2000b). Following that reasoning, we suggest that the spreading of LSW plays an important role in setting intermediate and deep $^{129}$I values of the SPNA (**Figure 5A**). For example, $^{129}$I concentrations increased more than 10 ×$10^7$ at/kg at depths occupied by $LSW_{new}$ in the Irminger Sea. And the eastward tracer increases delimited by the 5 ×$10^7$ at/kg contour line possibly indicates the transport of older and tracer-poorer LSW.

To further explore if $^{129}$I could unveil off-boundary pathways of LSW beyond the SPNA (turquoise dotted lines in **Figure 5B**) we visited three sites in the western and eastern subtropical North Atlantic Ocean (Figs. 5C and 5D). In the subtropical region, consistently with the literature, we preferred to call $NADW_U$ and $NEADW_U$ the water-masses derived from LSW far from its formation region, and $NADW_L$ for DSOW. To the best of our knowledge, the tracer observations presented here for BATS (**Figure 5C**) constitute the first full-depth profile of $^{129}$I in the low latitude North Atlantic aside from the two full depth profiles measured off the North American Slope in 1993/1994 (Santschi et al., 1996). In their $^{129}$I dataset, a near bottom tracer peak could be

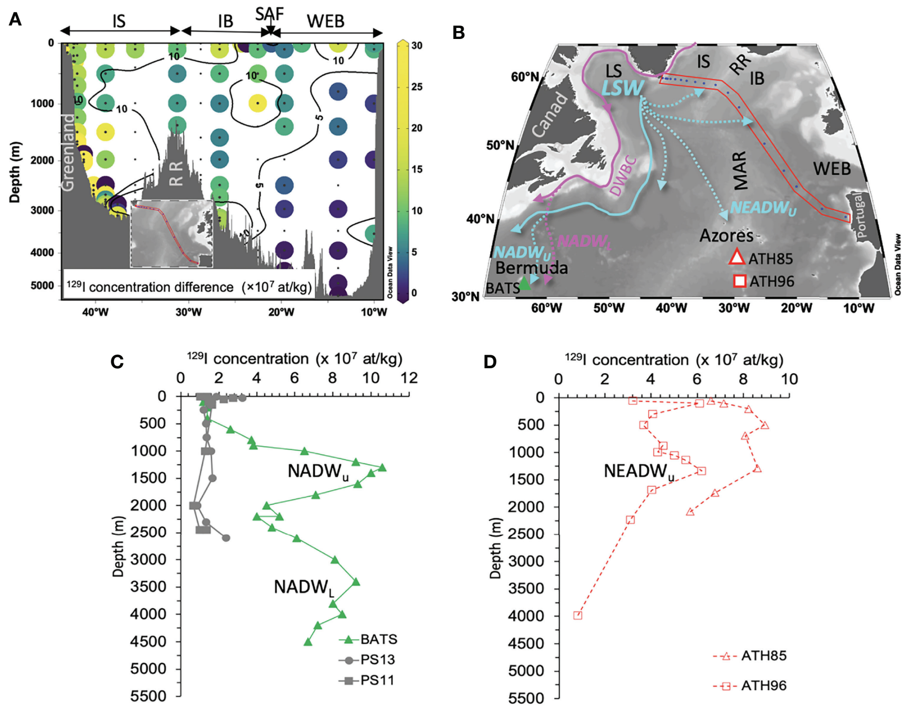


**FIGURE 5** | **(A)** Temporal change of $^{129}$I concentrations along the OVIDE line between 2014 (Castrillejo et al., 2018) and 2018 (this study) estimated as the subtraction of 2014 tracer values from 2018 observations overlapping at similar locations. **(B)** Map with the section plotted in **(A)** and the location of $^{129}$I depth profiles at **(C)** BATS and **(D)** ATHENA stations in the subtropical North Atlantic. Plot **(C)** includes the two $^{129}$I depth profiles sampled in 1993-1994 near the northeastern American slope at stations 13 (PS13, 36.3981°N, 74.2358°E) and 11 (PS11, 36.5081°N, 74.0908°E) reported by Peter H. Santschi et al. (1996). Acronyms in figure: Deep Western Boundary Current, (DWBC); Iceland Basin, (IB); Irminger Sea, (IS); Labrador Sea, (LS); Labrador Sea Water, (LSW); Mid Atlantic Ridge, (MAR); North Atlantic Deep Water, (NADW); North East Atlantic Deep Water, (NEADW); Reykjanes Ridge, (RR); Sub-Arctic Front, (SAF); and West European Basin, (WEB).

observed associated to the transport of $NADW_L$ *via* the Deep Western Boundary Current (**Figure 5C**). More recently another study by Smith et al. (2016) focused on the off-boundary transport of the same lower branch in our study area east of Bermuda (magenta dotted lines in **Figure 5B**). But they did not report $^{129}$I values for shallower depths occupied by $NADW_U$. In our BATS profile (**Figure 5C**) we observed a very clear peak of $^{129}$I centered at about 1500 m depth coinciding with potential densities ($\sigma_\theta$ ~27.75 kg/m$^3$, see **Table S1**) and a local salinity minimum (S~35) that characterize the LSW in the North Atlantic (McCartney and Talley, 1982). This tracer peak at 1500 m depth therefore shows that $^{129}$I data allow the straightforward identification of $NADW_U$ taking off-boundary pathways near Bermuda (turquoise dotted lines in **Figure 5B**). We also sampled two partial depth profiles south of the Azores Archipelago during ATHENA (**Figure 5D**). This far east $^{129}$I concentrations were lower than at BATS. The depths occupied by the $NEADW_U$ only showed slightly more elevated $^{129}$I concentrations at station ATH95 and a little further south at ATH96 the ~1500 m depth tracer peak could not be recognized. We learnt from other transient tracer observations, i. e. chlorofluorocarbons (CFCs), that highest fractions of LSW in the subtropical region are found in the DWBC and that the presence of young vintages is very limited east of the Mid Atlantic Ridge (e. g. Rhein et al., 2015). The three $^{129}$I depth profiles in **Figures 5C, D** show an eastward decrease in tracer concentrations that generally agrees with the spreading of LSW (or $NEADW_U$) inferred from CFC tracer fields. Yet, more $^{129}$I data are certainly needed to alleviate the sampling gap between the western and eastern subtropical North Atlantic and to confirm the relationship between the tracer distribution and the spreading of intermediate waters in the subtropical gyre.

The new $^{129}$I observations presented here show that deep ventilation in the subpolar region plays an important role on the sequestration of the tracer from shallow to deeper water layers supporting the modelling work of Orre et al. (2010) and Snyder, Aldahan and Possnert et al. (2010). While $^{129}$I has been used to infer mixing and transport timescales of DSOW in the SPNA (Smith et al., 2005) and down to Bermuda (Santschi et al., 1996; Smith et al., 2016), no published work has used $^{129}$I for investigating LSW or ISOW advection yet. This work clearly demonstrates that $^{129}$I is now being supplied at unprecedented rate (**Figure 5A**) through the Greenland-Scotland passages making more northern water masses traceable in the North Atlantic and that measurable tracer peaks extend at least as far as 30°N (**Figures 4, 5C**). The tracer intrusion in the North Atlantic shows that LSW and the overflows commonly take off-boundary pathways in agreement with drifting float (Bower et al., 2009; Bower et al., 2019) and CFC observations (Rhein et al., 2015). The clarity of $^{129}$I peaks captured at the stations sampled afar from the boundary regions (**Figures 4**, **5C**) indicates that recirculation through interior pathways must be important for the southward lower limb of the AMOC. Deflections of LSW and ISOW off the boundary currents appear to be related to latitudinal and meridional displacements of the North Atlantic Current (Bower et al., 2009; Bower and Furey, 2017; Xu et al., 2018) and its deep-reaching eddies and meanders (e.g., Zou et al., 2020). The partition between northern and southern waters also depends on the positioning of the North Atlantic Current, with southern (northern) waters with low (high) $^{129}$I concentrations generally occupying the regions east (west) of the main North Atlantic Current front. In this regard, a higher density sampling of $^{129}$I across North Atlantic Current boundaries in the subtropical and subpolar North Atlantic may be of interest to further investigate the driving forces of LSW and ISOW pathways. We think that the findings presented here are encouraging for the radionuclide tracer community. And thus, we call for a larger effort to build continued $^{129}$I time series which can help us better understand the structure and spreading rates of the AMOC.

## DATA AVAILABILITY STATEMENT

The original contributions presented in the study are included in the article/**Supplementary Material**. Further inquiries can be directed to the corresponding author. The iodine-129 data from the OVIDE 2018 cruise are available at SEANOE (Lherminier et al., 2022).

## AUTHOR CONTRIBUTIONS

MC collected the samples during OVIDE 2018 cruise and processed all seawater samples, he led the interpretation of data and the drafting of the manuscript. MC also raised part of the funds. NC managed the seawater sampling of PE424, BATS and ATHENA cruises, raised part of the funds for research and conducted the AMS measurements of iodine isotopes together with CV. PL led the OVIDE 2018 cruise facilitating the collection of samples and assessed the physical oceanographic aspects discussed in this work. All authors contributed to the article and approved the submitted version.

## FUNDING

The research of MC was partly funded by the ETH Career Seed Grant (SEED-06 19-2) and the Swiss National Science Foundation Postdoc Mobility Program (P400P2_199289). NC's funding came from the European Research Council (ERC Consolidator GAP-101001451) and the Swiss National Science Foundation (AMBIZIONE PZ00P2_154805 and PRIMA PR00P2_193091). The participation in the OVIDE 2018 Cruise onboard *R/V Thalassa* (https://doi.org/10.17600/18000510) was supported by PL and funds from the Laboratory of Ion Beam Physics. Support to process samples from PE424 cruise onboard *R/V* Pelagia and to participate on BATS monitoring onboard R/V Atlantic Explorer came from Swiss National Science Foundation Ambizione grant of NC. Funding for ATHENA Cruise (M151) onboard *R/V Meteor* came from Deutsche Forschungsgemeinschaft. The analysis of long-lived isotopes of iodine was possible thanks to internal funds of the Laboratory of Ion Beam Physics at ETH-Zurich and its consortium partners EAWAG, EMPA, and PSI. Open access funding provided by ETH Zürich.

## ACKNOWLEDGMENTS

Captains, crew and scientific staff of the four cruises are thanked for their dedication in collecting the samples used in this study. Thanks go to A. M. Wefing for her assistance in sample collection and comments on the manuscript and to A. Schlatter and K. Kündig for help in the laboratory. Norbert Frank is thanked for inviting us to participate in cruise ATHENA (M151). Acknowledgements go to Loes Gerringa and Rob Middag (NIOZ) who collected samples during the PE424 cruise. Rod Johnson (BIOS) and Anita Schlatter (EAWAG) collected the $^{129}$I profile during one of their monitoring cruises at BATS station. The analysis of waters masses would not have been possible without the hydrographic data that was kindly produced by different groups from many nationalities, thus, a big thank you to all. The constructive comments from the two reviewers are greatly appreciated.

## SUPPLEMENTARY MATERIAL

The Supplementary Material for this article can be found online at: https://www.frontiersin.org/articles/10.3389/fmars.2022.897729/full#supplementary-material

## REFERENCES

Alfimov, V., Aldahan, A., and Possnert, G. (2004). Tracing Water Masses With $^{129}$I in the Western Nordic Seas in Early Spring 2002. *Geophys. Res. Lett.* 31 (19), 10–13. doi: 10.1029/2004GL020863

Alfimov, V., Aldahan, A., and Possnert, G. (2013). "Water Masses and $^{129}$I Distribution in the Nordic Seas" in *Nuclear Instruments and Methods in Physics Research, Section B: Beam Interactions with Materials and Atoms.* Elsevier. pp. 542–546. doi: 10.1016/j.nimb.2012.07.042

Beaird, N. L., Rhines, P. B., and Eriksen, C. C. (2013). Overflow Waters at the Iceland–Faroe Ridge Observed in Multiyear Seaglider Surveys. *J. Phys. Oceanogr.* 43 (11), 2334–2351. doi: 10.1175/JPO-D-13-029.1

Bower, A., and Furey, H. (2017). Iceland-Scotland Overflow Water Transport Variability Through the Charlie-Gibbs Fracture Zone and the Impact of the North Atlantic Current. *J. Geophys. Res.: Oceans* 122 (9), 6989–7012. doi: 10.1002/2017JC012698

Bower, A. S., le Cann, B., Rossby, T., Zenk, W., Gould, J., Speer, K., et al. (2002). Directly Measured Mid-Depth Circulation in the Northeastern North Atlantic Ocean. *Nature* 419 (6907), 603–607. doi: 10.1038/nature01078

Bower, A., Lozier, S., Biastoch, A., Drouin, K., Foukal, N., Furey, H., et al. (2019). Lagrangian Views of the Pathways of the Atlantic Meridional Overturning Circulation. *J. Geophys. Res.: Oceans* 124 (8), 5313–5335. doi: 10.1029/2019JC015014

Bower, A. S., Lozier, M. S., Gary, S. F., and Böning, C. W. (2009). Interior Pathways of the North Atlantic Meridional Overturning Circulation. *Nature* 459 (7244), 243–247. doi: 10.1038/nature07979

Broecker, W. S., and Peng, T. H. (1982). *Tracers in the Sea* (Palisades, New York: Eldigio Press).

Casacuberta, N., Christl, M., Vockenhuber, C., Wefing, A. M., Wacker, L., Masqué, P., et al. (2018). Tracing the Three Atlantic Branches Entering the Arctic Ocean With $^{129}$I and $^{236}$U. *J. Geophys. Res.: Oceans* 123 (9), 6909–6921. doi: 10.1029/2018JC014168

Castrillejo, M., Casacuberta, N., Christl, M., Vockenhuber, C., Synal, H.-A., García-Ibáñez, M. I., et al. (2018). Tracing Water Masses With 129I and $^{236}$U in the Subpolar North Atlantic Along the GEOTRACES GA01 Section. *Biogeosciences* 15, 5545–5564. doi: 10.5194/bg-2018-228

Chang, Y. S., Garraffo, Z. D., Peters, H., and Özgökmen, T. M. (2009). Pathways of Nordic Overflows From Climate Model Scale and Eddy Resolving Simulations. *Ocean Model.* 29 (1), 66–84. doi: 10.1016/j.ocemod.2009.03.003

Christl, M., Vockenhuber, C., Kubik, P. W., Wacker, L., Lachner, J., Alfimov, V., et al. (2013). The ETH Zurich AMS Facilities: Performance Parameters and Reference Materials. *Nucl. Instruments Methods Phys. Res. Section B.: Beam Interact. Mater. Atoms* 294, 29–38. doi: 10.1016/j.nimb.2012.03.004

Clarke, R. A., and Gascard, J.-C. (1983). The Formation of Labrador Sea Water. Part I: Large-Scale Processes. *J. Phys. Oceanogr.* 13 (10), 1764–1778. doi: 10.1175/1520-0485(1983)013<1764:TFOLSW>2.0.CO;2

Daniault, N., Mercier, H., Lherminier, P., Sarafanov, A., Falina, A., Zunino, P., et al. (2016). The Northern North Atlantic Ocean Mean Circulation in the Early 21st Century. *Prog. Oceanogr.* 146, 142–158. doi: 10.1016/j.pocean.2016.06.007

Devana, M. S., Johns, W. E., Houk, A., and Zou, S. (2021). Rapid Freshening of Iceland Scotland Overflow Water Driven by Entrainment of a Major Upper Ocean Salinity Anomaly. *Geophys. Res. Lett.* 48, (22). doi: 10.1029/2021GL094396

Dickson, R. R., and Brown, J. (1994). The Production of North Atlantic Deep Water: Sources, Rates, and Pathways. *J. Geophys. Res.* 99 (C6), 12319. doi: 10.1029/94JC00530

Edmonds, H. N., Zhou, Z. Q., Raisbeck, G. M., Yiou, F., Kilius, L., and Edmond, J. M. (2001). Distribution and Behavior of Anthropogenic $^{129}$I in Water Masses Ventilating the North Atlantic Ocean. *J. Geophys. Res.: Oceans* 106 (C4), 6881–6894. doi: 10.1029/1999jc000282

Fleischmann, U., Hildebrandt, H., Putzka, A., and Bayer, R. (2001). Transport of Newly Ventilated Deep Water From the Iceland Basin to the Westeuropean Basin. *Deep-Sea Res. I* 48. doi: 10.1016/S0967-0637(00)00107-2

García-Ibáñez, M. I., Pérez, F. F., Lherminier, P., Zunino, P., Mercier, H., and Tréguer, P. (2018). Water Mass Distributions and Transports for the 2014 GEOVIDE Cruise in the North Atlantic. *Biogeosciences* 15 (7), 2075–2090. doi: 10.5194/bg-15-2075-2018

Gómez-Guzmán, J. M., Villa, M., le Moigne, F., López-Gutiérrez, J. M., and García-León, M. (2013). AMS Measurements of $^{129}$I in Seawater Around Iceland and the Irminger Sea. *Nucl. Instruments Methods Phys. Res. Section B.: Beam Interact. Mater. Atoms* 294, 547–551. doi: 10.1016/j.nimb.2012.07.045

Hansen, B., and Østerhus, S. (2007). Faroe Bank Channel Overflow 1995–2005. *Prog. Oceanogr.* 75 (4), 817–856. doi: 10.1016/j.pocean.2007.09.004

He, P., Aldahan, A., Possnert, G., and Hou, X. L. (2013a). "A Summary of Global $^{129}$I in Marine Waters" in *Nuclear Instruments and Methods in Physics Research, Section B: Beam Interactions with Materials and Atoms*. Berlin, Germany: Springer Nature 537–541. doi: 10.1016/j.nimb.2012.08.036

He, P., Hou, X., Aldahan, A., Possnert, G., and Yi, P. (2013b). Iodine Isotopes Species Fingerprinting Environmental Conditions in Surface Water Along the Northeastern Atlantic Ocean. *Sci. Rep.* 3, 1–8. doi: 10.1038/srep02685

Hou, X. (2004). Application of 129 I as an Environmental Tracer. *J. Radioanal. Nucl. Chem.* 262 (1), 67–75.

Lankhorst, M., and Zenk, W. (2006). *Lagrangian Observations of the Middepth and Deep Velocity Fields of the Northeastern Atlantic Ocean*. American Meteorological Society. doi: 10.1175/JPO2869.1

Lherminier, P., Perez Fiz, F., Branellec, P., Mercier, H., Velo, A., Messias, M. -J., et al. (2022). GO-SHIP A25 - OVIDE 2018 Cruise Data. *SEANOE*. doi: 10.17882/87394

McCartney, M. S., and Talley, L. D. (1982). The Subpolar Mode Water of the North Atlantic Ocean. *J. Phys. Oceanogr.* 12 (11), 1169–1188. doi: 10.1175/1520-0485(1982)012<1169:TSMWOT>2.0.CO;2

Orre, S., Smith, J. N., Alfimov, V., and Bentsen, M. (2010). Simulating Transport of $^{129}$I and Idealized Tracers in the Northern North Atlantic Ocean. *Environ. Fluid Mech.* 10 (1), 213–233. doi: 10.1007/s10652-009-9138-3

OSPAR (2015). *OSPAR Data & Information Management System. 2015* (United Kingdom: OSPAR Liquid Discharges from Nuclear Installations- 2015). Available at: https://odims.ospar.org/en/search/?datastream=liquid_discharges.

Perez, F. F., Fontela, M., García-Ibáñez, M. I., Mercier, H., Velo, A., Lherminier, P., et al. (2018). Meridional Overturning Circulation Conveys Fast Acidification to the Deep Atlantic Ocean. *Nature* 554 (7693), 515–518. doi: 10.1038/nature25493

Petit, T., Mercier, H., and Thierry, V. (2018). First Direct Estimates of Volume and Water Mass Transports Across the Reykjanes Ridge. *J. Geophys. Res.: Oceans* 123 (9), 6703–6719. doi: 10.1029/2018JC013999

Piron, A., Thierry, V., Mercier, H., and Caniaux, G. (2017). Gyre-Scale Deep Convection in the Subpolar North Atlantic Ocean During Winter 2014–2015. *Geophys. Res. Lett.* 44 (3), 1439–1447. doi: 10.1002/2016GL071895

Racapé, V., Thierry, V., Mercier, H., and Cabanes, C. (2019). ISOW Spreading and Mixing as Revealed by Deep-Argo Floats Launched in the Charlie-Gibbs Fracture Zone. *J. Geophys. Res.: Oceans* 124 (10), 6787–6808. doi: 10.1029/2019JC015040

Raisbeck, G. M., and Yiou, F. (1999). $^{129}$I in the Oceans: Origins and Applications. *Sci. Total Environ.* 237–238, 31–41. doi: 10.1016/S0048-9697(99)00122-9

Rhein, M., Kieke, D., and Steinfeldt, R. (2015). Advection of North Atlantic Deep Water From the Labrador Sea to the Southern Hemisphere. *J. Geophys. Res. C.: Oceans* 120 (4), 2471–2487. doi: 10.1002/2014JC010605

Santschi, P. H., Schink, D. R., Corapcioglu, O., Oktay-Marshall, S., Fehn, U., and Sharma, P. (1996). Evidence for Elevated Levels of Iodine-129 in the Deep Western Boundary Current in the Middle Atlantic Bight. *Deep Sea Res. Part I Oceanogr. Res. Pap.* 43, 2 59–265. doi: 10.1016/0967-0637(96)00005-2

Saunders, P. M. (1994). The Flux of Overflow Water Through the Charlie-Gibbs Fracture Zone. *J. Geophys. Res.* 99 (C6), 12343. doi: 10.1029/94JC00527

Schink, D. R., Santschi, P. H., Corapcioglu, O., and Fehn, U. (1995). Prospects for Iodine-129 Dating of Marine Organic Matter Using AMS. *Nucl. Instruments Methods Phys. Res. B.* 99, 524–527. doi: 10.1016/0168-583X(94)00695-4

Schott, F., Stramma, L., and Fischer, J. (1999). Interaction of the North Atlantic Current With the Deep Charlie Gibbs Fracture Zone Throughflow. *Geophys. Res. Lett.* 26 (3), 369–372. doi: 10.1029/1998GL900223

Sherwin, T. J., Griffiths, C. R., Inall, M. E., and Turrell, W. R. (2008). Quantifying the Overflow Across the Wyville Thomson Ridge Into the Rockall Trough. *Deep Sea Res. Part I.: Oceanogr. Res. Papers* 55 (4), 396–404. doi: 10.1016/j.dsr.2007.12.006

Smith, J. N., Jones, E. P., Moran, S. B., Smethie, J. M., and Kfieser, W. E. (2005). Iodine 129/CFC 11 Transit Times for Denmark Strait Overflow Water in the Labrador and Irminger Seas. *J. Geophys. Res. C.: Oceans* 110 (5), 1–16. doi: 10.1029/2004JC002516

Smith, J. N., McLaughlin, F. A., Smethie, W. M., Moran, S. B., and Lepore, K. (2011). Iodine-129, 137Cs, and CFC-11 Tracer Transit Time Distributions in the Arctic Ocean. *J. Geophys. Res.: Oceans* 116 (4), 1–19. doi: 10.1029/2010JC006471

Smith, J. N. Jr, Smethie, W. M., Yashayev, I., Curry, R., and Azetsu-Scott, K. (2016). Time Series Measurements of Transient Tracers and Tracer-Derived Transport in the Deep Western Boundary Current Between the Labrador Sea and the Subtropical Atlantic Ocean at Line W. *J. Geophys. Res.: Oceans*, 121, 1–14. doi: 10.1002/2015JC011486.Received

Snyder, G., Aldahan, A., and Possnert, G. (2010). Global Distribution and Long-Term Fate of Anthropogenic $^{129}$I in Marine and Surface Water Reservoirs. *Geochem. Geophysics Geosystems* 11 (4), 1–19. doi: 10.1029/2009GC002910

UK Environmental Agency (2015). *Radioactivity in Food and the Environment (RIFE) Reports. 2015* (United Kingdom: RIFE -2015). Available at: https://www.gov.uk/government/publications/radioactivity-in-food-and-the-environment-rife-reports.

van Aken, H. M. (2000a). The Hydrography of the Mid-Latitude Northeast Atlantic Ocean I: The Deep Water Masses. *Deep-Sea Res. I* 47, 757–788. doi: 10.1016/S0967-0637(99)00092-8

van Aken, H. M. (2000b). The Hydrography of the Mid-Latitude Northeast Atlantic Ocean II: The Intermediate Water Masses. *Deep Sea Res. Part I.:*

*Oceanographic Res. Papers* 47 (5), 789–824. doi: 10.1016/S0967-0637(99)00112-0

Vivo-Vilches, C., López-Gutiérrez, J. M., Periáñez, R., Marcinko, C., le Moigne, F., McGinnity, P., et al. (2018). Recent Evolution Of $^{129}$I Levels in the Nordic Seas and the North Atlantic Ocean. *Sci. Total Environ.* 621, 376–386. doi: 10.1016/j.scitotenv.2017.11.268

Vockenhuber, C., Casacuberta, N., Christl, M., and Synal, H. A. (2015). Accelerator Mass Spectrometry of $^{129}$I Towards its Lower Limits. *Nucl. Instruments Methods Phys. Res. Section B.: Beam Interact. Mater. Atoms* 361, 445–449. doi: 10.1016/j.nimb.2015.01.061

Wagner, M. J. M., Dittrich-Hannen, B., Synal, H.-A., Suter, M., and Schotterer, U. (1996). Increase of $^{129}$I in the Environment. *Nucl. Instruments Methods Phys. Res. Section B.: Beam Interact. Mater. Atoms* 113 (1–4), 490–494. doi: 10.1016/0168-583X(95)01348-2

Wefing, A.-M., Christl, M., Vockenhuber, C., van der Loeff, M.R., and Casacuberta, N. (2018). Tracing Atlantic Waters Using $^{129}$I and $^{236}$U in the Fram Strait in 2016. *J. Geophys. Res.: Oceans*. 124, 882–896. doi: 10.1029/2018JC014399

Wong, G. T. F. (1991). The Marine Geochemistry of Iodine. *Rev. Aquat. Sci.* 4, 45–73.

Xu, X., Bower, A., Furey, H., and Chassignet, E. P. (2018). Variability of the Iceland-Scotland Overflow Water Transport Through the Charlie-Gibbs Fracture Zone: Results From an Eddying Simulation and Observations. *J. Geophys Res.: Oceans* 123 (8), 5808–5823. doi: 10.1029/2018JC013895

Xu, X., Schmitz, W. J., Hurlburt, H. E., Hogan, P. J., and Chassignet, E. P. (2010). Transport of Nordic Seas Overflow Water Into and Within the Irminger Sea: An Eddy-Resolving Simulation and Observations. *J. Geophys Res.: Oceans* 115, (12). doi: 10.1029/2010JC006351

Yashayaev, I., Bersch, M., and van Aken, H. M. (2007). Spreading of the Labrador Sea Water to the Irminger and Iceland Basins. *Geophys Res. Lett.* 34 (10), L10602. doi: 10.1029/2006GL028999

Yashayaev, I., and Loder, J. W. (2016). Recurrent Replenishment of Labrador Sea Water and Associated Decadal-Scale Variability. *J. Geophys Res.: Oceans* 121 (11), 8095–8114. doi: 10.1002/2016JC012046

Yiou, F., Raisbeck, G. M., Zhou, Z. Q., and Kilius, L. R. (1994). $^{129}$I From Nuclear Fuel Reprocessing; Potential as an Oceanographic Tracer. *Nucl. Inst. Methods Phys. Res. B.* 92 (1–4), 436–439. doi: 10.1016/0168-583X(94)96050-X

Zou, S., Bower, A., Furey, H., Susan Lozier, M., and Xu, X. (2020). Redrawing the Iceland–Scotland Overflow Water Pathways in the North Atlantic. *Nat. Commun.* 11 (1), 1–8. doi: 10.1038/s41467-020-15513-4

Zou, S., Lozier, S., Zenk, W., Bower, A., and Johns, W. (2017). Observed and Modeled Pathways of the Iceland Scotland Overflow Water in the Eastern North Atlantic. *Prog. Oceanography* 159, 211–222. doi: 10.1016/j.pocean.2017.10.003

**Conflict of Interest:** The authors declare that the research was conducted in the absence of any commercial or financial relationships that could be construed as a potential conflict of interest.

**Publisher's Note:** All claims expressed in this article are solely those of the authors and do not necessarily represent those of their affiliated organizations, or those of the publisher, the editors and the reviewers. Any product that may be evaluated in this article, or claim that may be made by its manufacturer, is not guaranteed or endorsed by the publisher.